ISIJ International, Vol. 51 (2011), No. 12, pp. 1974–1981

Effect of Sulfur on the TTT Diagram of $CaO–Al_2O_3$ Slag at Eutectic Composition

Yoshiaki KASHIWAYA,[1)] Yasuaki KUSADA[2)] and Ryosuke O. SUZUKI[3)]

1) Graduate School of Energy Science and Technology, Kyoto University, Yoshida Honmachi, Sakyoku, Kyoto, 606-8501 Japan. 2) Formerly Graduate Student, Graduate School of Eng., Hokkaido University. Now at Nippon Steel Corporation. Ohita Works, Nishi-no-su, Ohita, 870-0992 Japan. 3) Graduate School of Eng., Faculty of Engineering, Hokkaido University. Kita-13Jou, Nishi-8Choume, Kita-ku, Sapporo, Hokkaido, 060-8628 Japan.

(*Received on May 13, 2011; accepted on July 21, 2011*)

It is important to know the behavior of inclusion in a $CaO–Al_2O_3$-(SiO_2 and/or MgO) system for controlling the properties of steel. The crystallization of inclusion has a large effect on the rolling process. However, there is little study of the effect of sulfur on the crystallization of inclusion. In the previous paper, the authors were investigated the sulfur behavior in the $CaO–Al_2O_3$ slag at the eutectic composition (CA_{EU}) under controlled atmosphere. In the present study, the effects of sulfur on the TTT diagrams were measured by the hot thermocouple method under controlled atmosphere. 1 mass%, 5 mass% and 10 mass% CaS were added to the eutectic composition of calcium aluminate (CA_{EU}).

The crystal region in TTT diagrams was expanded by the addition of CaS from 1 mass% to 10 mass% under Ar atmosphere. And the start of crystallization became faster with the increase of CaS addition. The crystal phases were monocalcium aluminate (CA) and tricalcium aluminate (C_3A) regardless to the CaS content. However, primary crystal was changed from the content of CaS. When 1 mass%CaS was added to CA_{EU}, the primary crystal was CA. On the other hand, the primary crystal was C_3A in the cases of 5 mass% and 10 mass%CaS.

KEY WORDS: TTT diagram; desulfurization slag; hot thermocouple; crystallization.

1. Introduction

The influence of the reduction of CO_2 emission in the iron and steelmaking field can be effective on the total reduction of Japanese CO_2 emission. Among the countermeasures for saving the resources and energy, a recycle and reuse of slags are one of the effective ways, because the slags contain many kinds of elements and have a high temperature around 1 500°C, when it is exhausted. There are many kinds of slags depending on the purpose which makes the recycle of slags difficult. A desulfurization slag is also difficult to use for a landfilling or roadbed material. To promote the recycle of the desulfurization slags, it is important to know the physicochemical properties of the slag.

Furthermore, it is important to know the behavior of inclusion in a $CaO–Al_2O_3$-(SiO_2 and/or MgO) system for controlling the properties of steel. Numata, *et al.*[1)] have studied the composition change of inclusion in $CaO–Al_2O_3$–CaS system during addition of Ca alloy and $CaO–Al_2O_3$ flux. Zhao, *et al.*[2)] have studied the crystallization of inclusion in $CaO–Al_2O_3–SiO_2$ system with the basicity of 0.9. However, there is no data on the crystallization of an inclusion in terms of sulfur content.

In the previous paper,[3)] the authors were investigated the sulfur behavior in the $CaO–Al_2O_3$ slag at the eutectic composition (CA_{EU}). The sulfur in CA_{EU} is easy to react with oxygen in atmosphere (Eq. (1)).

$$\mathrm{CaS\ (in\ slag)} + \frac{3}{2}\mathrm{O_2\,(g)} \rightarrow \mathrm{CaO\ (in\ slag)} + \mathrm{SO_2\,(g)} \quad (1)$$

The sulfur added hardly remained in the slag. Then, the atmosphere controlled hot thermocouple method[4–6)] was developed for decreasing the oxygen potential (P_{O_2}) and increasing the sulfur potential (P_{SO_2}) in the atmosphere.

In this study, the effect of sulfur content on the TTT diagram of CA_{EU} slag using hot thermocouple technique under controlled atmosphere. The effect of sulfur on the mechanism of crystallization of CA_{EU} slag was clarified.

2. Experimental

The experimental method and procedure are the same as the previous study.[3)] The composition of a mother slag at the eutectic point (CA_{EU}: 64.2 mol%CaO-35.8 mol%Al_2O_3, **Fig. 1**)[7–10)] was selected. In this experiment, a large amount of the mother slag of CaO-35.8 mol%Al_2O_3 was made and a mixing of CaS was carried out using the same mother slag.

A reagent CaS was added to the mother slag. The CaS additions were 1 mass%, 5 mass% and 10 mass%, which were expressed as CA_{EU}-S1, CA_{EU}-S5 and CA_{EU}-S10, respectively. The sulfur contents in the slag were 0.35 mol%S, 1.75 mol%S, 3.55 mol%S, respectively. Those compositions are summarized in **Table 1**. In addition, an atmosphere was controlled by a titanium plate and CaS pellet on a titanium plate as shown by the previous study.[3)] The

Table 1. Composition of sample slag used and atmosphere.

	CaO mol% (mass%)	Al_2O_3 mol% (mass%)	CaS mol% (mass%)	S mol% (mass%)	Atmosphere		
					Ar	Ar-Ti	Ar-Ti-CaS
CA_{EU}	64.2 (49.7)	35.8 (50.3)	0.00	0.00	○	○	○
CA_{EU}-S1	63 6 (49.2)	35.4 (49.8)	1.00 (1.00)	0.35 (0.44)	○	–	–
CA_{EU}-S5	61.0 (47.2)	34.0 (47.8)	5.02 (5.00)	1.75 (2.22)	○	–	–
CA_{EU}-S10	57.8 (44.7)	32.2 (45.3)	10.0 (10.0)	3.55 (4.44)	○	○	○
CA_{EU}-CaO	67.8 (53.7)	32.2 (46.3)	0.00	0.00	○	–	–

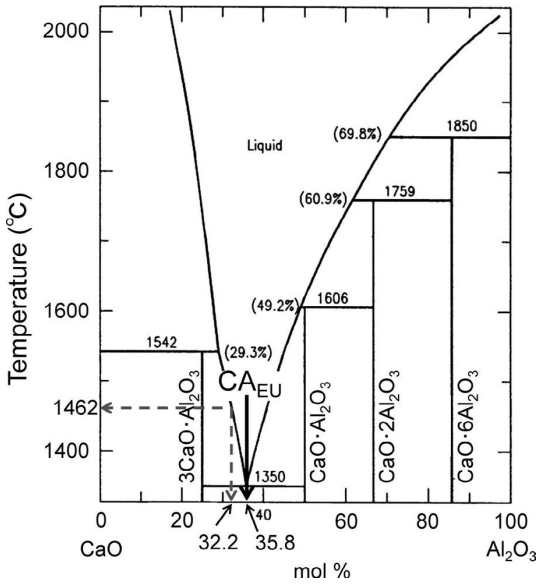

Fig. 1. Phase diagram of CaO–Al_2O_3 system and composition of mother slag.

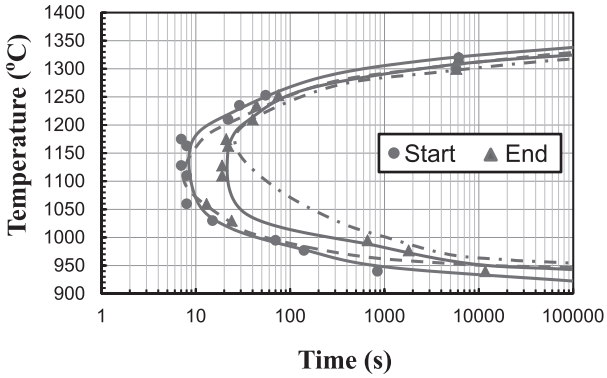

Fig. 2. TTT diagram of CA_{EU} –S1 (1 mass%CaS) under Ar atmosphere.

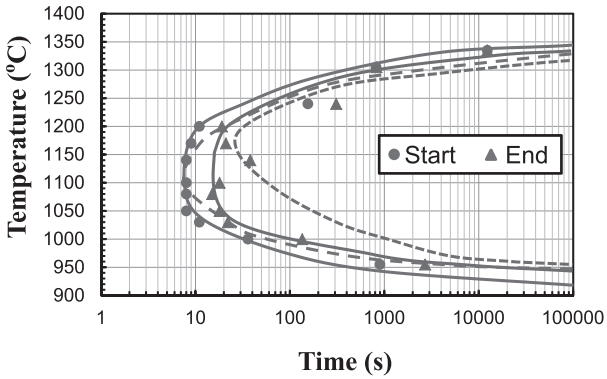

Fig. 3. TTT diagram of CA_{EU} –S5 (5 mass%CaS) under Ar atmosphere.

differences of atmosphere were denoted by Ar, Ar–Ti and Ar–Ti–CaS (Table 1). The equilibrium partial pressure of oxygen for the reaction of titanium oxidation ($Ti+O_2(g)=TiO_2$) is 10^{-15}Pa at 1 405°C.[3] In this experiment, the sample melt was quenched from 1 550°C to the respective temperatures from 1 300°C to 900°C for the measurement of TTT diagram, while the temperature of Ti plate was about 800°C. It was considered that the actual oxygen partial pressure could be less than 10^{-15}Pa around the Ti plate.

As mention above, some of CaS added was oxidized by oxygen in gas phase (Eq. (1)). If a complete oxidation of CaS was done, CaO content would increase. In the case of CA_{EU}-S10, the composition will change to 67.7 mol%CaO-32.2 mol%Al_2O_3. And the position in the equilibrium diagram (Fig. 1) also indicated by the broken arrows. For comparison of the results of CA_{EU}-S10, 3.6 mol% (4 mass%) CaO was added to the mother slag (CA_{EU}) in the assumption of the complete oxidation. The notation of the sample was CA_{EU}-CaO as shown in Table 1.

3. Results and Discussions

3.1. Effects of Sulfur Content on TTT Diagram

Figure 2 shows the TTT diagram of CA_{EU}-S1 (1 mass%CaS added) obtained under Ar atmosphere. The solid circles and line mean the start of crystallization, and the solid triangles and line mean the end of crystallization. In addition, the dashed line and the dotted and dashed line means the start and the end of crystallization for CA_{EU} obtained in the previous study.[3] The nose position of CA_{EU}-S1 is about 7 s and the temperature is from 1 050°C to 1 170°C. The start lines of crystallization between CA_{EU}-S1 and CA_{EU} are almost the same. In the temperature range higher than the nose point, the start and end lines are overlapped, which means the quite high rate of crystallization. Although the start of crystallization in the temperature range lower than the nose point is almost the same, the end of crystallization in CA_{EU}-S1 is about 150 s faster than that of CA_{EU}.

Figure 3 shows the TTT diagram of CA_{EU}-S5 (5 mass%CaS added) obtained under Ar atmosphere. The TTT diagram of CA_{EU}-S5 is quite resemble to CA_{EU}-S1, however, the start line of crystallization is slightly moved toward the earlier time of crystallization.

Figure 4 shows the TTT diagram of CA_{EU}-S10 (10 mass%CaS added) obtained under Ar atmosphere. When the addition of CaS increased to 10 mass% (4.44 mass%S), the

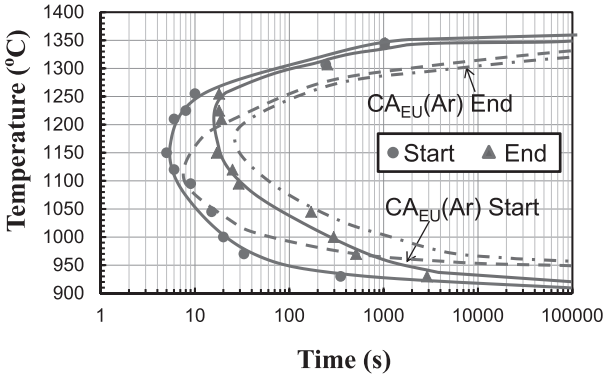

Fig. 4. TTT diagram of CA_{EU}–S10 (10 mass%CaS) under Ar atmosphere.

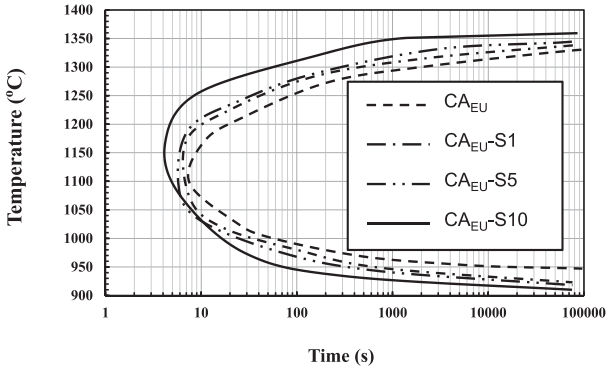

Fig. 5. Comparison of TTT diagrams among different sulfur contents in CA_{EU} under Ar atmosphere.

start and the end of crystallization were faster significantly, and the crystal region became large. The nose position of CA_{EU}-S10 is about 5 s at 1 170°C. At the temperature of 1 340°C, the start and the end of crystallization are almost the same and about 1 000 s, which is quite faster crystallization than that of CA_{EU}. In the case of CA_{EU}, the crystallization at the temperature higher than 1 330°C never occurred during the observation within 100 000 s (28 h). **Figure 5** shows the comparison of the starts of crystallization in TTT diagrams among CA_{EU}-S1, CA_{EU}-S5, CA_{EU}-S10 and CA_{EU} under Ar atmosphere. It was found that the addition of CaS makes the start of crystallization earlier, as a result, the crystal region of TTT diagram expands.

XRD analyses were performed to clarify the crystal phase precipitated at 1 300°C and the results were shown in **Fig. 6**. The crystal phases were almost the same and the monocalcium aluminate, CA($CaO{\cdot}Al_2O_3$) and tricalcium aluminate,C_3A($3CaO{\cdot}Al_2O_3$) for all sample, even if the temperature went down below the nose temperature (The detail was shown in the later section). Some example of the double nose TTT diagram was shown by Kashiwaya, *et al*.,[5] when a different two crystals precipitated. However, in this experiment, the two kinds of crystal were precipitated simultaneously. One of reason is that the rate of crystallization is quite fast (the start and the end lines of crystallization are almost overlapped). **Figure 7** shows the ΔG° of the reactions for $CaO{\cdot}Al_2O_3$ (Eq. (2)) and $3CaO{\cdot}Al_2O_3$ (Eq. (3)). It is found that the both crystals are stable enough in the high temperature range and the tricalcium aluminate (C_3A) is stabler than the monocalcium aluminate (CA). However, as mentioned above, the rate of crystallization was fast for the both crystals, which meant the diffusion(s) of CaO and/or Al_2O_3 would very fast, and there is little difference of rate of formation between CA and C_3A. From these reasons, the crystal region in TTT diagram are almost the same or overlapped each other.

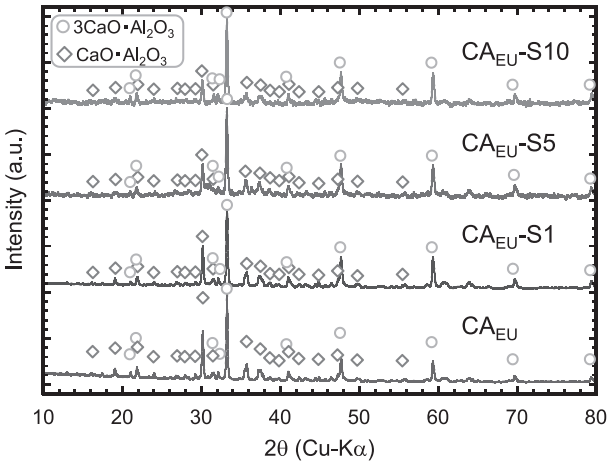

Fig. 6. Comparison of XRD patterns among different sulfur contents in CA_{EU} quenching from 1 300°C under Ar atmosphere.

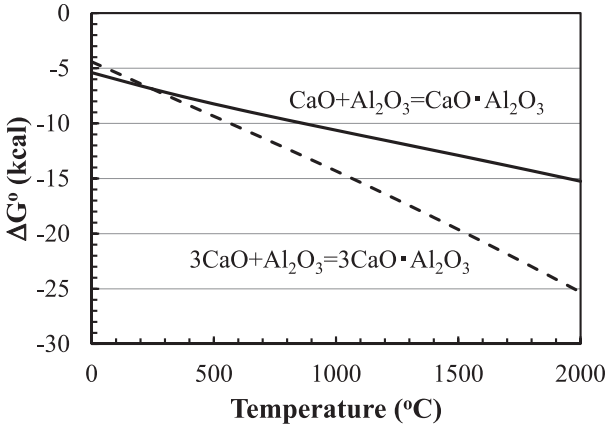

Fig. 7. ΔG° of reactions for monocalcium aluminate ($CaO{\cdot}Al_2O_3$) and tricalcium aluminate ($3CaO{\cdot}Al_2O_3$).

$$CaO+Al_2O_3=CaO{\cdot}Al_2O_3 \quad \text{..... (2)}$$

$$3CaO+Al_2O_3=3CaO{\cdot}Al_2O_3 \quad \text{..... (3)}$$

Moreover, there was no CaS peak found in the XRD patterns. It was considered that the content of sulfur was a little and some extent of oxidation reaction of CaS (Eq. (1)) would occur. The details will be discussed in the later section.

Figure 8 shows the results of SEM observation for CA_{EU} ((a), (b)) and CA_{EU}-S1((c), (d)) quenched from 1 300°C under Ar atmosphere. The microstructure of CA_{EU} shows a fine uniform eutectic structure. On the other hand, many plate like crystal of monocalcium aluminate (CA) were precipitated in the CA_{EU}-S1((c), (d)), which was resemble to the structure of CA_{EU} solidified under Ar–Ti atmosphere without sulfur.[3] In this case, the primary crystal was monocalcium aluminate (CA). The reaction mechanism can be considered as follows.

For the precipitation of the primary crystal:

$$CaS_{(l)}+O_{(in\ slag)} \rightarrow CaO^*_{(l)}+S_{(in\ slag)} \quad \text{..... (4)}$$

$$CaO^*_{(l)}+Al_2O_{3(l)} \rightarrow CA_{(primary\ crystal)} \quad \text{..... (5)}$$

For the solidification of eutectic structure;

$$CaO_{(l)}+Al_2O_{3(l)} \rightarrow CA_{EU} \quad \text{..... (6)}$$

The oxidation of CaS will be expressed by Eq. (4). The produced CaO, which is expressed as CaO*, can be make a nucleation site for the primary crystal of CA (Eq. (5)), since it should be distinguished from the original CaO. The formed CaO* might be active and could be nucleation site of the primary crystal of monocalcium aluminate, CA (a detailed discussion was done in the later section).

Figure 9 shows the comparison of SEM images between CA_{EU}-S5 ((a), (b)) and CA_{EU}-S10 ((c), (d)) quenched from

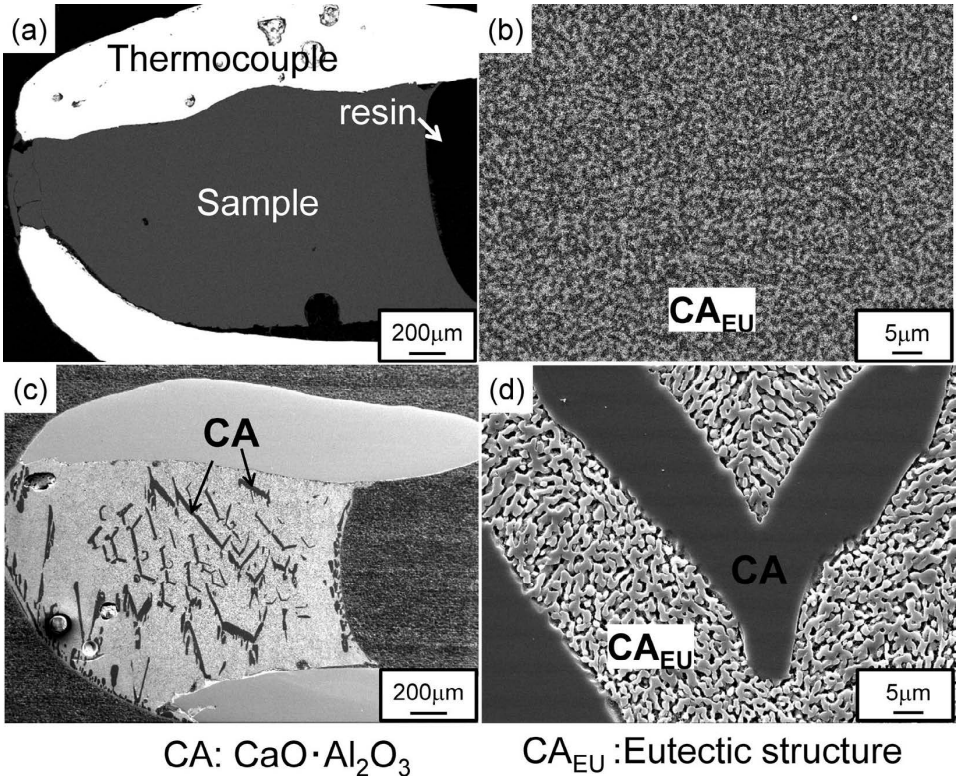

Fig. 8. Comparison of SEM images of CA_{EU} ((a), (b)) and CA_{EU}-S1 ((c), (d)) under Ar atmosphere.

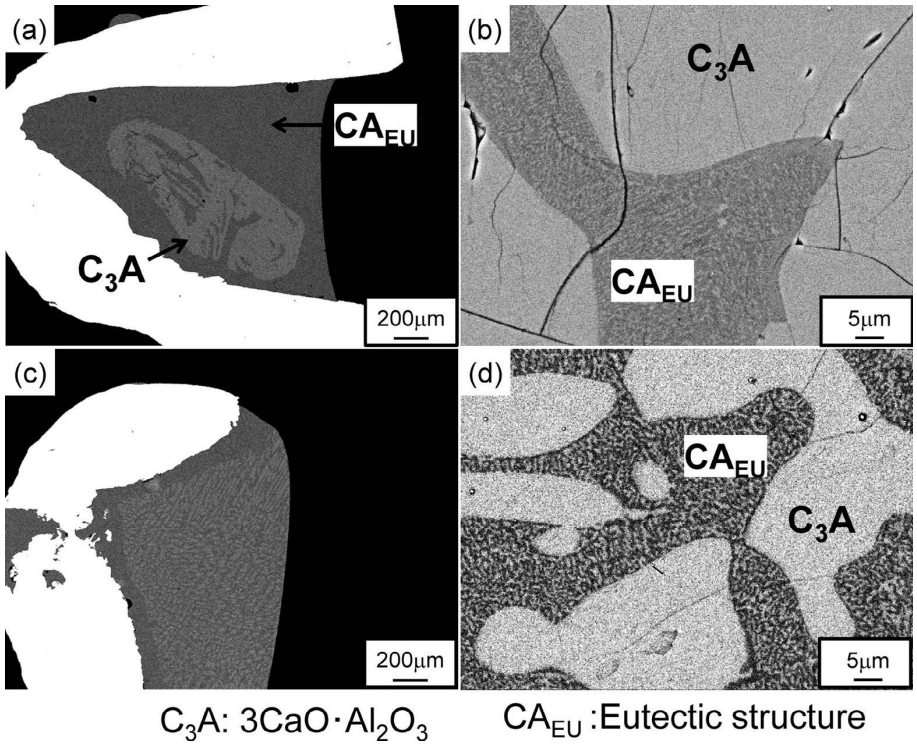

Fig. 9. Comparison of SEM images of CA_{EU}-S5 ((a), (b)) and CA_{EU}-S10 ((c), (d)) under Ar atmosphere.

1 300°C under Ar atmosphere. From 5 mass% of CaS addition, the primary crystal was changed to the tricalcium aluminate (C_3A). In the case of CA_{EU}-S5, the primary crystal of C_3A was segregated in the center of sample. It might be an irregular results coming from the sample mixing or oxidation reaction during experiment. Unfortunately, an extra-experiment could not be performed for confirming the reproducibility. However, it can be concluded that the primary crystal in CA_{EU}-S5 system is the tricalcium aluminate (C_3A) from the consistency of results of other data as shown in the later sections.

When 10 mass% CaS was added to the mother slag, many fine primary crystals of C_3A were precipitated throughout the sample (Fig. 9(c)). The shape of C_3A was dendritic. To estimate the amount of C_3A and CA, the ratios of intensities for the peak height of (440) of C_3A to (123) of CA in the different sulfur content of sample were plotted in **Fig. 10**. It was found that the linear relationship was obtained, when the addition of CaS increased from 1 mass% to 10 mass%. This result means that a some content of CaO will increase with the addition of CaS, however, when it is compared with the peak height ratio of CA_{EU}-CaO, in which the whole CaS added by 10 mass% is completely oxidized, the peak height ratio ($I_{(440)C3A}/I_{(123)CA}$) in the CaS addition is very low and the increased CaO content was estimated to about 0.5 mass%, which increased by the reaction of oxidation.

From above consideration, a consumption of CaS was very small and the most of CaS remain in the sample. However, it was very difficult to detect the existence of sulfur in the sample by EPMA, because it was a small quantity. If undissolved CaS existed in the sample melt, the detection of sulfur was relatively easy. When the sulfur dissolved in the CA and C_3A crystal structures, the unit cell of those crystals would expand. Then, the interplanar spaces of CA and C_3A were examined by XRD (CA: ICDD (The International Centre for Diffraction Data) 00-53-0191, monoclinic, two main peaks overlapped are (123)[d_{123}=29.6688 nm] and (220)[d_{220}= 29.5887 nm], C_3A: ICDD 00-038-1429, cubic, main peak is (440) [d_{440}=26.9874 nm]). In the case of monocalcium aluminate (CA), the peak at 30° (Cu-Kα) is an overlapped peaks of (123) and (220). In this paper, a notation of peak of (123) is representative one for the both peaks. In **Fig. 11**, the variations of interplanar spaces of $(123)_{CA}$ and $(440)_{C3A}$ v.s. CaS content are plotted. At 0 mass% CaS, the interplanar spaces of $(123)_{CA}$ and $(440)_{C3A}$ are 29.613 nm and 26.944 nm, respectively. The difference from the reference data of ICDD is an error of experiment, however, the variations of peak shift are the quite accurate values. It was found that both of the interplanar spaces increased with the content of CaS, although the proportions of expansion for CA and C_3A were 0.07% and 0.09%, respectively.

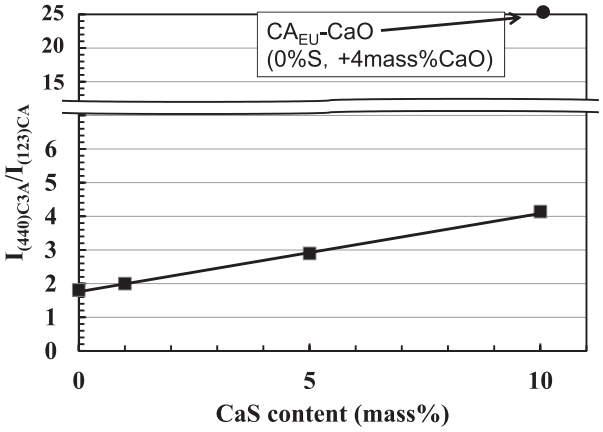

Fig. 10. Variation of peak height ratio of $(440)_{C3A}/(123)_{CA}$ among different sulfur contents in CA_{EU} quenching from 1 300°C under Ar atmosphere.

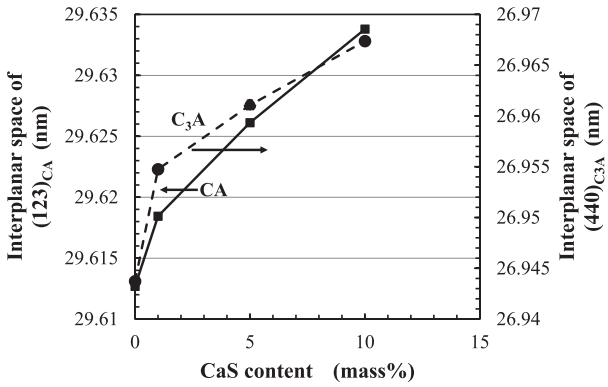

Fig. 11. Variation of Interplanar spaces of $(440)_{C3A}$ and $(123)_{CA}$ among different sulfur contents in CA_{EU} under Ar atmosphere.

3.2. TTT Diagrams of CA_{EU}-S10 under Ar and Ar–Ti–CaS

Figure 12 shows the TTT diagram of CA_{EU}-S10 under Ar–Ti–CaS atmosphere in comparison with the TTT diagram of CA_{EU} under Ar atmosphere. The solid circles means the start of crystallization and the solid triangles means the end of crystallization. The start of crystallization became fast especially in the temperature range higher than that of the point of nose, at which the starting time was about 5 s to 6 s in the wide temperature range from 1 050°C to 1 270°C. On the other hand, the nose point of CA_{EU} under Ar atmosphere (dashed line) was about 7 s at 1 100°C. A scattering of end of crystallization expressed by the solid triangles were large especially in the lower temperature range from 1 100°C to 970°C, which might come from the instability of the partial pressure of SO_2 in gas phase, although the details were not known at the present moment. Anyway, since the time from the start to the end of crystallization was very short, the rate of crystallization was quite fast in the whole crystal region.

Figure 13 shows the comparison of TTT diagrams among CA_{EU}-S10 under Ar–Ti–CaS, CA_{EU}-S10 under Ar and CA_{EU} under Ar. It was found that the crystal region became larger by the addition of CaS, significantly. In addition, although the difference of atmosphere between Ar–Ti–CaS and Ar atmospheres was relatively small, the crystal region under Ar–Ti–CaS was slightly expanded in the high temperature region.

Figure 14 shows the comparison of XRD patterns among CA_{EU}-S10 at 1 000°C under Ar, CA_{EU}-S10 at 1 300°C under Ar and CA_{EU} at 1 300°C under Ar. The temperature at 1 000°C means the region below the nose point and the one at 1 300°C means the region over the nose point. It can be said that the crystal phases in high temperature (1 300°C) and low temperature (1 000°C) are the same. The ratio

between $(123)_{CA}$ and $(440)_{C3A}$ of the main peaks is also the same. In **Fig. 15**, the microstructure of CA_{EU}-S10 at 1 000°C under Ar is shown. Quite fine dendritic structure, which consisted of C_3A, precipitated in the whole sample.

Figure 16 shows SEM images of CA_{EU}-S10 at 1 300°C under Ar–Ti–CaS atmosphere. Figs. 16(a) and 16(b) corresponds to the cross section of sample in the horizontal direction at the position of thermocouple, while Figs. 16(c) and 16(d) corresponds to the vertical section including the position of tip of thermocouple. These photos are to examine the difference of microstructure in the different positions,

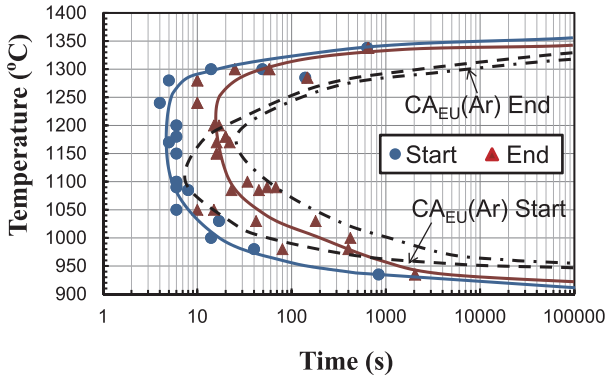

Fig. 12. TTT diagrams of CA_{EU}-S10 under Ar–Ti–CaS atmosphere in comparison with CA_{EU} under Ar atmosphere.

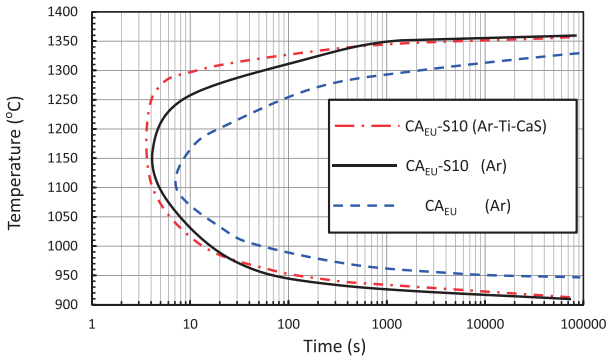

Fig. 13. Comparison of starting line of crystallization in TTT diagrams of CA_{EU}-S10 under different atmospheres (Ar and Ar+Ti+CaS).

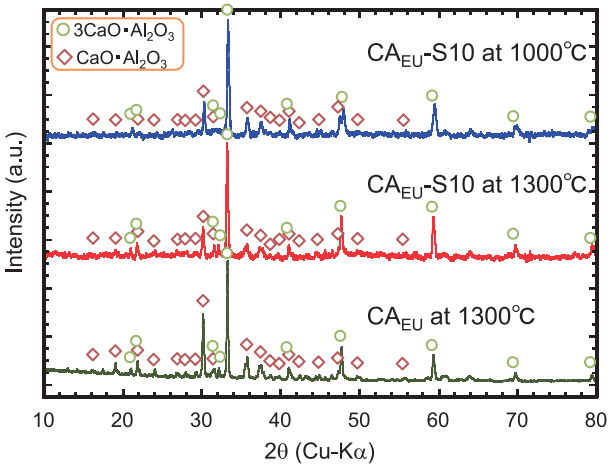

Fig. 14. XRD patterns of CA_{EU}-S10 at 1 000°C and 1 300°C in comparison of CA_{EU}.

because the partial pressure of SO_2 might differ from the position especially at the upper and the lower part of sample. As a result, relatively coarse dendritic C_3A was precipitated uniformly in the whole sample and there was little difference in the microstracture. However, an odd phenomenon was observed at the lower surface of sample shown as Fig. 16(c). The defected region might be caused from an abnormal surface tension by the sulfur or some compound of sulfide formed by a higher P_{SO2} coming from CaS pellet which set in the electric furnace. Unfortunately, no additional experiment could be performed. Further experiment will be performed for obtaining the equilibrium state in future.

Figure 17 shows the elements mapping and COMP image of EPMA on the sample of CA_{EU}-S10 at 1 300°C

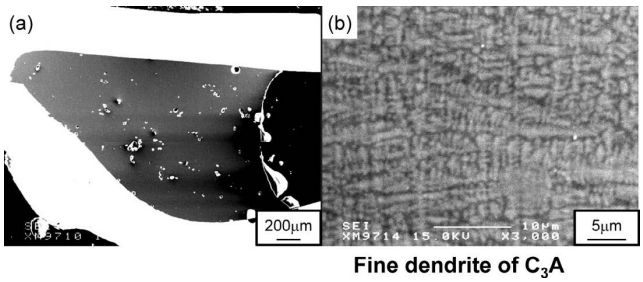

Fig. 15. CA_{EU}-S10 at 1 000°C under Ar atmosphere.

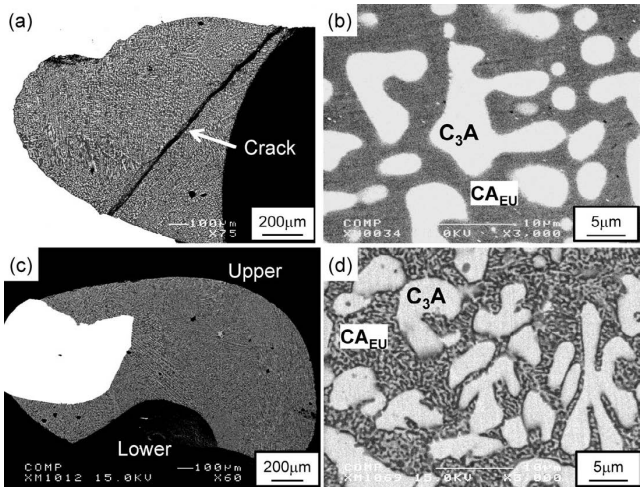

Fig. 16. SEM images of CA_{EU}-S10 at 1 300°C under Ar–Ti–CaS atmosphere. (a), (b) Horizontal section, (c), (d) Vertical section.

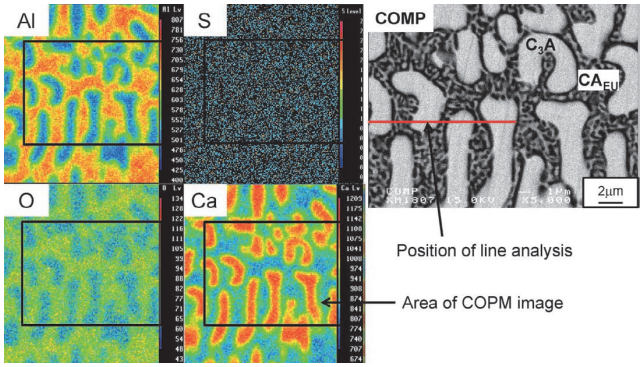

Fig. 17. Result of EPMA of CA_{EU}-S10 at 1 300°C under Ar–Ti–CaS atmosphere.

under Ar–Ti–CaS. It was found that the precipitated crystals were the dendrites of C_3A, however, the clear evidence of the existence of sulfur could not obtained by the mapping. Then, line analyses of S, Ca and Al were performed at the position shown in Fig. 17 (COMP). The results are shown in **Fig. 18**, where the higher position of CaO corresponds to the C_3A and the lower position means the eutectic structure (CA_{EU}). In this case, the existence of sulfur was clearly confirmed, and the position of sulfur concentrated was in the eutectic structure between C_3A dendrites. As mentioned above, it was found that some content of sulfur dissolved in the crystal structures of CA and C_3A according to the results of XRD. However, it might be small quantity of sulfur. Most of sulfur remained might be concentrated in the melt and finally in the eutectic structure of CA_{EU} during precipitation of C_3A.

3.3. TTT Diagram of CA_{EU}-CaO

As mentioned above, if a complete oxidation of 10%CaS added occurred, the increase of CaO was 4 mass% against CA_{EU} mother slag and the sample was notated as CA_{EU}-CaO. The TTT diagram of CA_{EU}-CaO was measured and compared with CA_{EU} in **Fig. 19**. The nose point of CA_{EU}-CaO was about 7 s at 1 200°C, which was about 100°C higher than that of CA_{EU}. The equilibrium melting point is 1 462°C at 67.8 mol%CaO-32.2 mol%Al_2O_3 (Fig. 1). In Fig. 19, the melting point will be expected over 1 400°C. In **Fig. 20**, the TTT diagram of CA_{EU}-CaO was compared with those of CA_{EU}-S10 under Ar–Ti–CaS and CA_{EU} under Ar. It was found that the high temperature region of CA_{EU}-CaO was significantly expanded, however, the low temperature region was almost the same with CA_{EU}. It can be said that the existence of sulfur affected the crystallization in a low temperature region, significantly.

Figure 21 shows the comparison of XRD patterns among CA_{EU}-CaO, CA_{EU}-S10 under Ar–Ti–CaS and CA_{EU} under Ar atmosphere at 1 300°C. Most of crystal phase in CA_{EU}-CaO was C_3A, however, the both of CA and C_3A precipitated in CA_{EU}-S10. These results are the one of evidence that no complete oxidation of 10 mass%CaS occurred and clearly a sulfur remained in the sample. **Figure 22** shows the SEM images of CA_{EU}-CaO. Large and dense crystals of C_3A dendrites were precipitated in the whole sample. The morphology of C_3A crystal is resemble to the one in CA_{EU}-S10, however, it is considered that the amount of C_3A is less than that in CA_{EU}-CaO. Moreover, the CaO just produced from the oxidation reaction of CaS would be more active than that of CaO added, then, the active CaO was expressed as CaO* as shown by Eqs. (5) and (4) and the reaction mechanisms were considered.

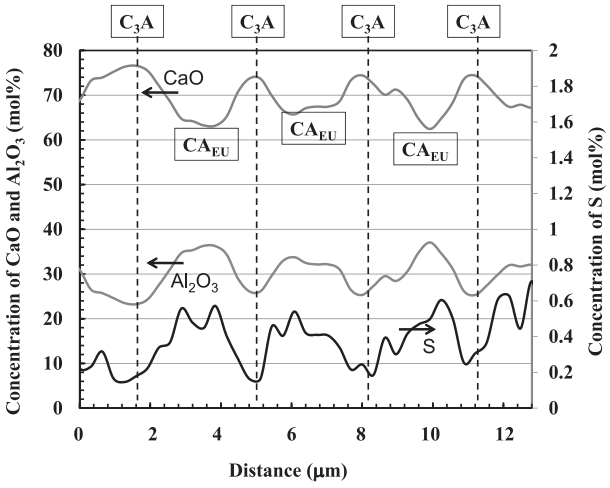

Fig. 18. Result of line analysis of CA_{EU}-S10 at 1 300°C under Ar–Ti–CaS atmosphere.

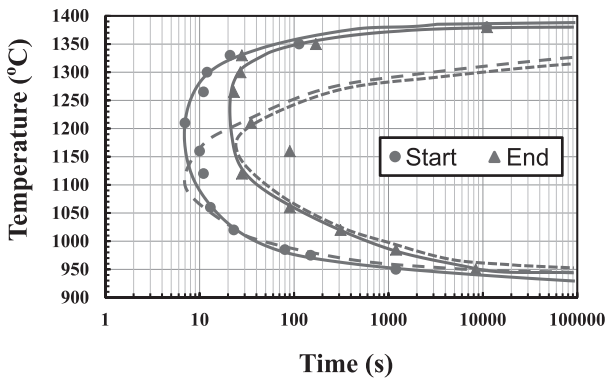

Fig. 19. TTT diagrams of CA_{EU}-CaO under Ar atmosphere in comparison with CA_{EU} under Ar atmosphere.

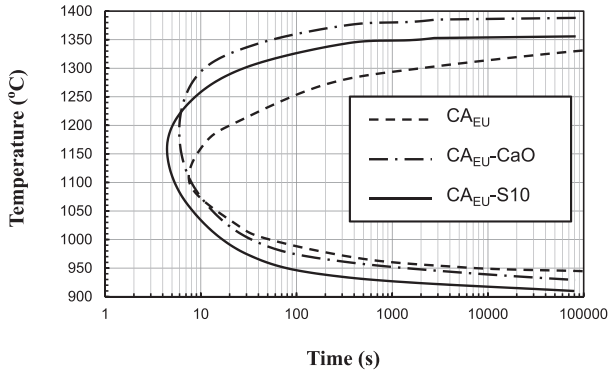

Fig. 20. Comparison of TTT diagrams among CA_{EU}-S10 under Ar–Ti–CaS atmosphere, CA_{EU}-CaO under Ar and CA_{EU} under Ar atmosphere.

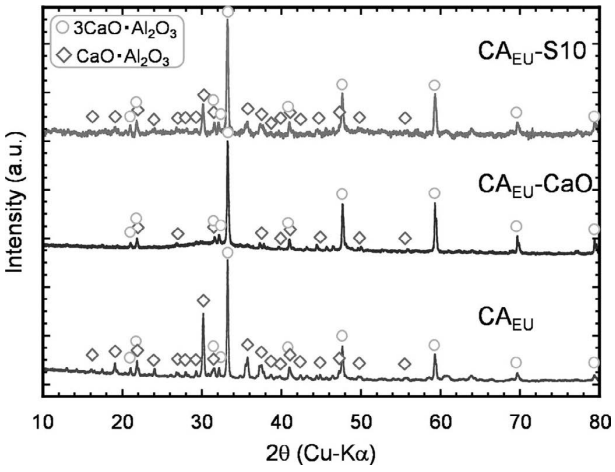

Fig. 21. Comparison of XRD patterns among CA_{EU}-S10 (Ar–Ti–CaS), CA_{EU}-CaO (Ar) and CA_{EU} (Ar) at 1 300°C.

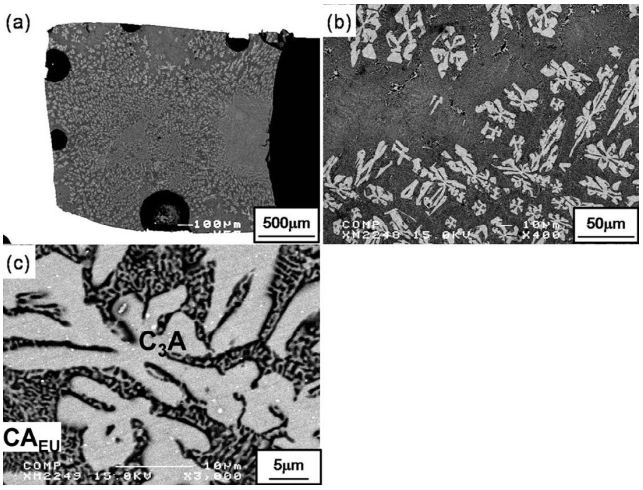

Fig. 22. SEM images of CA_{EU}-CaO at 1 300°C under Ar atmosphere.

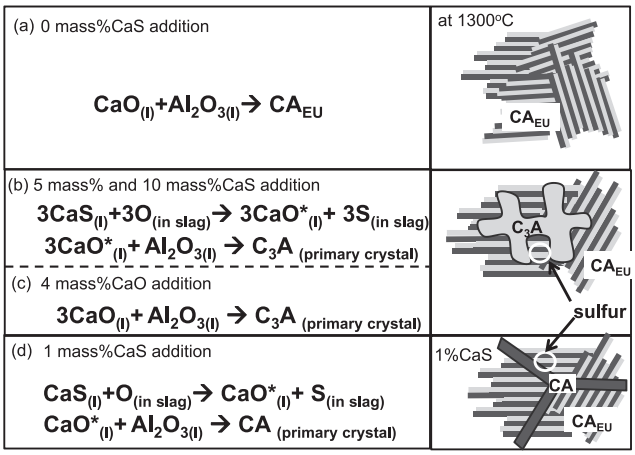

Fig. 23. Mechanisms of precipitation of primary crystal in the eutectic structure. (Sulfur dissolves in the both crystals of CA and C_3A. In addition, sulfur concentrates at the interface and the eutectic structure between the primary crystals).

3.4. Mechanisms of Precipitation of Primary Crystal

In **Fig. 23**, the mechanisms of precipitation of primary crystal are summarized in comparison with the solidification of eutectic structure of monocalcium aluminate (CA_{EU}). Eq. (6) shows the general solidification of CA_{EU} (Fig. 23(a)).

$$CaO_{(l)}+Al_2O_{3(l)} \rightarrow CA_{EU} \text{..... (6) again}$$

On the other hand, when CaS more than 5 mass% was added, the primary crystal is the tricalcium aluminate (C_3A) according to the Eqs. (7) and (8) as shown by Fig. 23(b).

$$3CaS_{(l)}+3O_{(\text{in slag})} \rightarrow 3CaO^*_{(l)}+3S_{(\text{in slag})} \text{..... (7)}$$

$$3CaO^*_{(l)}+Al_2O_{3(l)} \rightarrow 3CaO\cdot Al_2O_3\ _{(\text{primary crystal})} \text{..... (8)}$$

When 4 mass%CaO (CA_{EU}-CaO) was added to CA_{EU}, the reaction expressed by Eq. (9) occurred as shown by Fig. 23(c).

$$3CaO_{(l)}+Al_2O_{3(l)} \rightarrow 3CaO\cdot Al_2O_3\ _{(\text{primary crystal})} \text{..... (9)}$$

Finally, when 1 mass%CaS was added, the reactions expressed by Eqs. (4) and (5) could occur and the monocalcium aluminate (CA) was precipitated (Fig. 23(d)).

Although, some content of sulfur existed in the crystal structures of CA and C_3A, most of sulfur concentrated in the melt during the precipitation of the primary crystal and then, the sulfur existed in the eutectic structure.

4. Conclusions

Effects of sulfur on the TTT diagrams were measured by the hot thermocouple method under controlled atmosphere. 1 mass%, 5 mass% and 10 mass% CaS were added to the eutectic composition of calcium aluminate (CA_{EU}). The obtained results are as follows.

(1) The crystal region in TTT diagrams was expanded by the addition of CaS from 1 mass% to 10 mass% under Ar atmosphere. The start of crystallization became faster with the increase of CaS addition.

(2) The crystal phases were monocalcium aluminate (CA) and tricalcium aluminate (C_3A) regardless to CaS content. However, primary crystal was changed from the addition of CaS.

(3) When 1 mass%CaS was added to CA_{EU}, the primary crystal was CA. On the other hand, the primary crystal was C_3A in the cases of 5 mass% and 10 mass%CaS.

(4) The crystal region in TTT diagram of CA_{EU}-S10(10 mass% CaS addition) under Ar–Ti–CaS atmosphere expanded slightly in comparison with CA_{EU}-S10 under Ar atmosphere.

(5) Some content of sulfur existed in the crystal structures of CA and C_3A. While the most of sulfur concentrated in the melt and finally existed in the eutectic structure.

(6) The mechanisms of primary crystal precipitation according to the CaS additions were summarized and presented.

REFERENCES

1) M. Numata and Y. Higuchi: *Tetsu-to-Hagané*, **97** (2011), 259.
2) C. Zhao, S. M. Jung, Y. Kashiwaya, H. Gaye and H. G. Lee: *ISIJ Int.*, **48** (2008), 747.
3) Y. Kashiwaya, Y. Kusada and R. O. Suzuki: *ISIJ Int.*, **51** (2011), 1967.
4) Y. Kashiwaya, C. E. Cicutti, A. W. Cramb and K. Ishii: *ISIJ Int.*, **38** (1998), 348.
5) Y. Kashiwaya, C. E. Cicutti and A. W. Cramb: *ISIJ Int.*, **38** (1998), 357.
6) P. Kahn Son and Y. Kashiwaya: *ISIJ Int.*, **48** (2008), 1165.
7) B. R. W. Nurse, J. H. Welch and A. J. Majumdar: *Trans. Br. Ceram. Soc.*, **64** (1965), 409.
8) A. K. Chatterjee and G. I. Zhmoidin: *J. Mater. Sci.*, **7** (1972), 93.
9) G. Eriksson and A. D. Pelton: *Metall. Trans. B*, **24B** (1993) 807.
10) J. Jeevaratnam, F. P. Glasser and L. S. Dent Glasser: *J. Amer. Soc.*, **42** (1964), 105.